**Research article**

**SDR9C7 catalyzes critical dehydrogenation of acylceramides for skin barrier formation**

Takeichi T, et al.

## Supplemental Methods

**Whole-exome sequencing**.

Blood samples from the patient and her parents for genetic testing were obtained in accordance with the Declaration of Helsinki. Following informed consent, genomic DNA from the proband was used for whole-exome sequencing. Exome capture was performed by in-solution hybridization using SureSelect Human All Exon V5 bait (Agilent Technologies, Santa Clara, CA, USA). Massively parallel sequencing was performed with the Illumina HiSeq2500 platform with 150-bp paired end-reads (Illumina, San Diego, CA). The reads produced were aligned to the hg19 reference human genome using the Burrows-Wheeler Aligner software with default parameters and a –mem option (1). PCR duplicates were removed using MarkDuplicates in Picard tools (https://broadinstitute.github.io/picard/). Candidate variants were called using VarScan2 (http://massgenomics.org/varscan) and annotated using ANNOVAR (http://annovar.openbioinformatics.org/). Common variants defined by >1% minor allele frequency in ExAC (http://exac.broadinstitute.org/), 1000 genomes (http://www.1000genomes.org/), or ESP6500 (http://evs.gs.washington.edu/EVS/) were excluded from analysis.

**Electron microscopy.**

Neonatal mouse skin samples were fixed in 2.5% (w/v) glutaraldehyde solution, post-fixed in 0.5% (w/v) ruthenium tetroxide ($RuO_4$), dehydrated and embedded in Epon812 (TAAB Laboratories, Berks, UK). All the samples were ultra-thin sectioned at a thickness of 75 nm, and stained with uranyl acetate and lead citrate. Photographs were taken using a JEM1400 transmission electron microscope (JEOL Ltd., Tokyo, Japan).

**Skin permeability assays.**

Toluidine blue staining of newborn mice was described previously (2). In brief, newborns were anesthetized, dehydrated in methanol, washed in PBS and stained for 30 min in 0.1% (w/v) toluidine blue/PBS (3). After washing in PBS, the pups were photographed. TEWL was measured using a VAPO SCAN AS-VT100RS (Asahi Techno Lab.ltd., Yokohama, Japan). Measurements were performed after calibration of the device at room temperature with minimized influence of air turbulence, and the results were recorded when the TEWL values were stabilized 30–45 s after probe placement.

**Microarray and real-time quantitative PCR**.

Total RNA extracted from P0 newborns (n=5, each group) with TRIzol (Thermo Fisher) was purified using a RNeasy Mini Kit (QIAGEN). For DNA microarray, equal amounts of total RNA pooled from five mice for each genotype were used. The quality of RNA was assessed with a 2100 Bioanalyzer (Agilent Technologies). Fluorescently labelled antisense RNA (cRNA targets) were synthesized with a Low Input QuickAmp Labeling Kit according to the manufacturer's protocol (Agilent Technologies). Samples were hybridized to the Mouse Gene Expression 4x44K v2 Microarray (G4846A, Agilent Technologies), washed, and then scanned using a SureScan Microarray Scanner (Agilent Technologies). Microarray data were analysed with Feature Extraction software (Agilent Technologies) and then imported into GeneSpring GX 14.9 software (Agilent Technologies). Signal intensities were normalized by global normalization. The microarray data can be accessed at the GEO repository under the accession numbers GSE87682 (3) and GSE135643.

For real-time qPCR, total RNA was reverse-transcribed into cDNA using ReverTra Ace qPCR RT Master Mix (Toyobo) in accordance with the manufacturer's instructions. qPCR reactions were performed on a LightCycler480-II (Roche) using THUNDERBIRD Probe

qPCR Mix (Toyobo). The sequences of primers designed to be compatible with the Roche Universal Probe Library (UPL) are provided in Supplemental Table 11. A total of 2 µl cDNA was used for the quantification of endogenous mRNA levels. Expression levels were normalized to *Hprt1*.

**Preparation of oxidized linoleates and deuterated internal standards.**

9- and 13-hydroperoxyoctadecadienoic acids (HPODE) and the corresponding hydroxy-octadecadienoates (HODE) were prepared by enzymatic synthesis of the R or S enantiomers or by autoxidation to the racemates as described (4). 9*R*,10*R*-*trans*-epoxy-11*E*-13*R*-hydroxyoctadecenoate or the racemate were produced by hematin treatment of 9*R*-HPODE or 9*RS*-HPODE, respectively (4). 9*R*,10*S*,13*R*-trihydroxy-11*E*-octadecenoate was prepared by total chemical synthesis, and authentic 9*R*,10*S*-dihydroxy-11*E*-13-keto-octadecenoate as the 9,10-acetonide was available as an intermediate in the total synthesis (5). The free acid of 9*R*,10*S*-dihydroxy-11*E*-13-keto-octadecenoate was also prepared by hydrolysis of 9*R*,10*R*-*trans*-epoxy-11*E*-13-keto-octadecenoate with recombinant soluble epoxide hydrolase.

9*R*,10*R*-*trans*-epoxy-11*E*-13-keto-octadecenoate was prepared by the sequence: oxygenation of linoleic acid by soybean lipoxygenase; reduction of the 13-hydroperoxide with sodium borohydride; oxidation of 13-HODE as the methyl ester (diazomethane) to 13-keto-octadeca-9*Z*,11*E*-dienoate with TPAP (DCM, 5 min on ice) (6); iodine-induced isomerization to the 9-*trans*,13-*trans* isomer, 13-keto-octadeca-9*E*,11*E*-dienoate (7); selective epoxidation of the 9*E* (*trans*) double bond using meta-chloroperoxybenzoic acid (mCBPA) (8) to produce the racemate of the target compound; resolution of the 9*R*,10*R*-*trans*-epoxy-11*E*-13-keto and 9*S*,10*S*-*trans*-epoxy-11*E*-13-keto enantiomers using a Chiralpak AD column with hexane/EtOH/MeOH (100:5:5, v/v/v) as solvent (9). All intermediates and final product in the sequence were purified and characterized by HPLC, UV, and $^{1}$H-NMR.

The deuterated internal standards of 9-HODE, 9*R*,10*R*-*trans*-epoxy-11*E*-13*R*-hydroxy-octadecenoate, and the 9*R*,10*S*,13*R*-triol for LC-MS quantitative assays were prepared from [9,10,12,13-$^{2}H_4$]linoleic acid (Cayman Chemical) as described (10). The deuterated internal standards for assay of 9*R*,10*R*-*trans*-epoxy-11*E*-13-keto-octadecenoate was prepared by derivatization of the free acid with trideuterated methoxylamine hydrochloride $CD_3ONH_2.HCl$ (CDN Isotopes, Quebec, Canada) in pyridine for 2 h at room temperature followed by extraction and separation of the syn and anti methoxime isomers by normal phase HPLC. The second eluting isomer with (λmax 245 nm in EtOH) was quantified assuming a molar extinction coefficient of 12,500 $M^{-1}$ $cm^{-1}$ and used to spike epidermal extracts after their derivatization with unlabeled methoxylamine hydrochloride. Similarly, trideuterated methoxime derivative of 9*R*,10*S*-dihydroxy-11*E*-13-keto-octadecenoate was prepared and used for assays of the corresponding 9,10-dihydroxy-13-ketone in epidermal extracts.

**Quantitative LC-MS analysis of oxidized linoleate-containing ceramides in murine epidermis.**

Neonatal pups were euthanized by decapitation, the skin removed and treated overnight at 4°C with Dispase. The epidermis was then teased apart, blotted dry, weighed and stored at -80°C prior to extraction and LC-MS analysis. For lipid extraction, the epidermal samples (weighing 20 – 30 mg) were placed in individual 5 ml glass Reactivials (Thermo-Fisher Scientific) in 3 ml MeOH/$CHCl_3$ (1:1, v/v) and kept at -20°C overnight under argon. The samples were diced with sharp scissors into small pieces and homogenized using a Sonic Dismembrator Model 100 with a 2 mm diameter probe (Fisher Scientific) on a setting of 3. The

probe was rinsed with an additional 1 ml solvent, and the combined extract was centrifuged at 2500 x g for 15 min in a Beckman-Coulter Allegra X12R centrifuge, the solvent collected and the protein pellet extracted three more times as above. The resulting protein pellet was resuspended in MeOH/$CHCl_3$ (1:1, v/v) and stored at -80°C for subsequent analysis of covalently bound ceramides. The pooled MeOH/$CHCl_3$ extracts were taken to dryness at room temperature under a stream of nitrogen, resuspended in 4 ml $CHCl_3$, and immediately after addition of 4 ml hexane loaded onto a 0.5 g silica extraction cartridge (Agilent); the open-bed column was washed with hexane/$CHCl_3$ (not collected) followed by collection of the elute using 16 ml of $CHCl_3$/MeOH (2:1, v/v).

At this stage half of each extract was kept in reserve and the other half transferred to a 2 ml Eppendorf tube, taken to dryness under $N_2$, and treated with 100 µl methoxylamine hydrochloride (10 mg/ml in pyridine) overnight at room temperature under argon. To recover the lipids while avoiding exposure of linoleate allylic epoxides to acidic conditions (as occurs by direct evaporation of the pyridine containing methoxylamine.HCl), 1 ml $CHCl_3$ was added and the samples extracted twice with 0.5 ml 0.1 M $K_2HPO_4$ and once with water and the upper aqueous layers discarded. The $CHCl_3$ phase was taken to dryness and a mixture of the following deuterated internal standards added in 10 µl MeOH: 0.1 nmole (30 – 35 ng), d4-9-HODE, d4-9*R*,10*R*-epoxy-11*E*-13*R*-hydroxy-octadecenoate, d3-methoxime of 9*R*,10*R*-*trans*-epoxy-11*E*-13-keto-octadecenoate, d3-methoxime of 9*R*,10*S*-dihydroxy-11*E*-13-keto-octadecenoate, and d4-9*R*,10*S*,13*R*-Triol. Alkaline hydrolysis of esterified lipids was then carried out by addition of 100 µl 10% MeOH, 275 µl MeOH, and 125 µl 2N KOH in 20% water in MeOH with shaking overnight at room temperature under argon (10). On the following day 455 µl CHCl3 and 393.5 µl water were added (thus approximating the proportions of a Bligh and Dyer extraction (11)), the samples vigorously mixed, briefly centrifuged and the lower phase removed using a 0.5 ml glass Hamilton syringe and discarded. The upper alkaline phase containing the potassium salts of the oxidized fatty acids was re-extracted using 0.5 ml theoretical lower phase (prepared by mixing solvents in the Bligh and Dyer proportions) and again the lower phase was removed and discarded. The volume of the upper phase was reduced to approximately 0.2 ml by evaporation under $N_2$, then 1.8 ml water was added and the still strongly alkaline sample applied to a preconditioned 1 ml Oasis cartridge. After washing with water until the eluate was neutral (this occurs within 1 ml of water wash), the oxidized linoleates and deuterated internal standards were eluted using 1 ml EtOAc. Subsequently the pentafluorobenzyl (PFB) esters were prepared for LC-MS analysis, and half of the sample was further derivatized to the dimethoxypropyl (DMP) acetonide derivative for LC-MS analysis of linoleate triols as described (10).

The PFB or PFB-DMP derivatives were analyzed as the M-PFB ions by APCI-LC-MS using a TSQ Vantage instrument (Thermo Scientific) with the APCI vaporizer temperature set to 500 °C, and the capillary temperature set to 150 °C. The HPLC used a Waters Alliance 2690 system and a Phenomenex Luna 5 µ silica column (25 x 0.2 cm) with a flow rate of 0.6 ml/min, and a solvent of hexane/isopropanol in the proportions 100:0.2 (v/v) for analysis of 9-HODE (recorded at m/z 295 (d0) and 299 (d4)), 9,10-epoxy-13-hydroxy-C18:1 (m/z 311 and 315), 9,10-epoxy-13-methoxime-C18:1 (m/z 338 and 341 (d3)), 9,10-dihydroxy DMP 13-methoxime (m/z 396 and 399 (d3)) and the proportions 100:1 (v/v) for analysis of linoleate triols (PFB, DMP derivative recorded at m/z 369 (d0) and 373 (d4)).

Quantitation of CerOS covalently-bound to epidermal proteins used the protein pellets from the above analysis and was carried out essentially as previously described (9) using a different LC-MS instrument. Briefly, after additional washes of the protein pellets with

MeOH/$CHCl_3$ (1:1, v/v) to remove non-covalently bound ceramides, the protein pellets were incubated in 1 M KOH in 95% methanol at room temperature overnight, and the ceramides released from ester linkage then recovered by Bligh and Dyer extraction. LC-MS analysis used a Waters Alliance 2695 Separations Module (Waters, Milford, MA) and an LTQ linear ion trap mass spectrometer (Thermo-Electron, San Jose, CA) equipped with an *Ion Max* APCI source. The APCI source was operated in positive ion mode, with full scan spectra (700–900 *m/z*) acquired using the following optimized parameters: $N_2$ sheath gas 50 psi; $N_2$ auxiliary gas 5 psi; APCI corona current 5 μA; APCI vaporizer temperature 275 °C; capillary temperature 300 °C; capillary offset 35 V; tube lens offset (at 800 *m/z*) 100 V; AGC target ion count $1e^4$; AGC max. inject time 10 ms. Data acquisition and quantitative spectral analysis were done using Thermo-Finnigan Xcalibur v. 2.0.7 SP1 and LTQ Tune v. 2.5.0. The samples for CerOS analysis were dissolved in the normal-phase LC solvent (hexane/isopropanol/glacial acetic acid, 90:10:0.1 v/v/v) and run isocratically on a Luna 5 μ silica column (25 x 0.2 cm) with a solvent of hexane/isopropanol/glacial acetic acid, 90:10:0.1 (v/v/v) at a flow rate of 0.6 ml/min, with retention time for CerOS of approximately 4 min.

**LC-MS screening of epidermal extracts for oxidized linoleate-containing ceramides.**

The total ion current profile (*m/z* 200–2000) of a MeOH/$CHCl_3$ extract of wild-type and *Sdr9c7*$^{-/-}$ murine epidermis was recorded using a Waters Alliance 2690 HPLC system coupled to a TSQ Vantage mass spectrometer (Thermo Scientific) with the APCI vaporizer temperature set to 500°C, and the capillary temperature set to 150 °C (9). The normal-phase HPLC system employed a Thomson Advantage 5μ silica column (250 x 4.6 mm) run with gradient elution of hexane/IPA/HAc (95:5:0.1) to hexane/IPA/HAc (75:25:0.1) over 30 min. Spectra were obtained on all peaks in the total ion current profile.

**Expression, purification, and assay of human and mouse SDR9C7.**

cDNA of full-length human *SDR9C7* was purchased from Kazusa Genome Technologies (Chiba, Japan). The substitution c.826C>T (p.Arg276Cys) is a novel mutation in the ARCI patient of the present study, whereas the truncation c.658C>T (p.Arg220*) is previously reported mutation in the patient with ARCI from another group (12). Human SDR9C7 proteins (wt, c.826C>T (p.Arg276Cys) and c.658C>T (p.Arg220*)) were expressed including an N-terminal FLAG tag in a silkworm-baculovirus system, ProCube (Sysmex Corporation, Kobe, Japan) as described elsewhere (13). Expression constructs of the mouse Sdr9c7 were synthesized by BioBasic (Amherst, New York), transferred into pET28b vector and expressed in *E. coli*; this produced strong enzymatic activity in the bacterial lysate (100 μl lysate/ml completely metabolized 100 μM 13-HODE free acid in 10 min at 37 °C); however, despite testing N-terminal and C-terminal $His_6$ tags in the constructs, the activity was not captured on a nickel affinity column; because of ester hydrolase activity in the crude lysate, these preparations were of limited utility for analysis of esterified substrates.

Enzyme incubations with FLAG tag-purified SDR9C7 were conducted at room temperature in a total volume of 0.5 ml in 0.1 M sodium phosphate pH 7.4 containing 1 mM NAD, 100 μM substrate (e.g. epoxy-hydroxy free fatty acid or methyl ester), 0.1 % polyoxyethylene tridecyl ether detergent (Sigma) and 1–2 μg enzyme. Rates of reaction were monitored by UV spectroscopy as appearance of the NADH chromophore (λmax 340 nm, recorded for 10 min by repetitive scans at 1 min intervals over the range 300–450 nm).

After continuing the incubation for 30 min at room temperature, enzymatic products were extracted with dichloromethane or using a 30 mg Oasis cartridge (Waters) with final elution using ethyl acetate or methanol. Initial screening of the products was conducted on an

Agilent 1200 series HPLC system with the diode array detector set to monitor 205, 220, 235 and 270 nm. Reversed-phase HPLC used a Waters Symmetry C18 column (25 x 0.46 cm) with isocratic solvent systems of acetonitrile/water/glacial acetic acid adjusted from 80:20:0.01 (v/v/v) to higher percentages of water depending on the polarity of the analytes, with a flow rate of 1 ml/min. Normal-phase HPLC used a Thompson Advantage silica column (25 x 0.46 cm) with solvent systems of hexane containing 0.5–5 % isopropanol, depending on the polarity of the analytes. Chiral HPLC used a Chiralpak AD column (15 x 0.2 cm, or 25 x 0.46 cm) with a solvent system of hexane/EtOH/MeOH for epoxy-hydroxy methyl ester derivatives (9).

## Supplemental Figures

### Supplemental Figure 1.

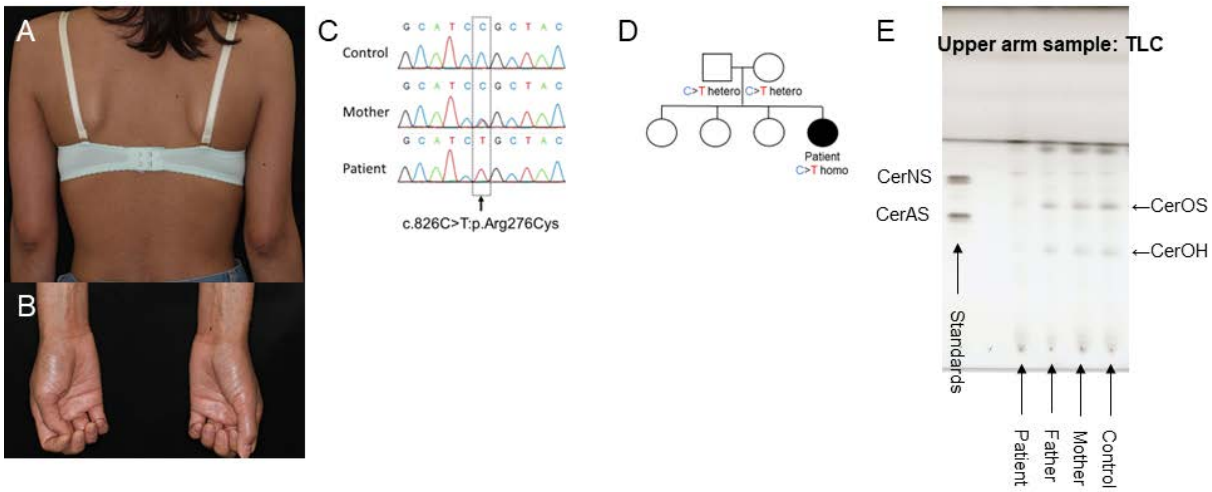


**Supplemental Figure 1. Clinical and pathological features of the patient.**
(A, B) Diffuse brown scales are seen on the back, the upper arms (A) and the lower leg (B). (C, D) Genomic sequencing revealed a c.826C>T transversion in the proband. Both the parents were found to have the heterozygous for the mutation. DNAs from the elder sisters were not available for testing. (E) Representative TLC analysis of lipids extracted from the skin of the participants.

**Supplemental Figure 2.**

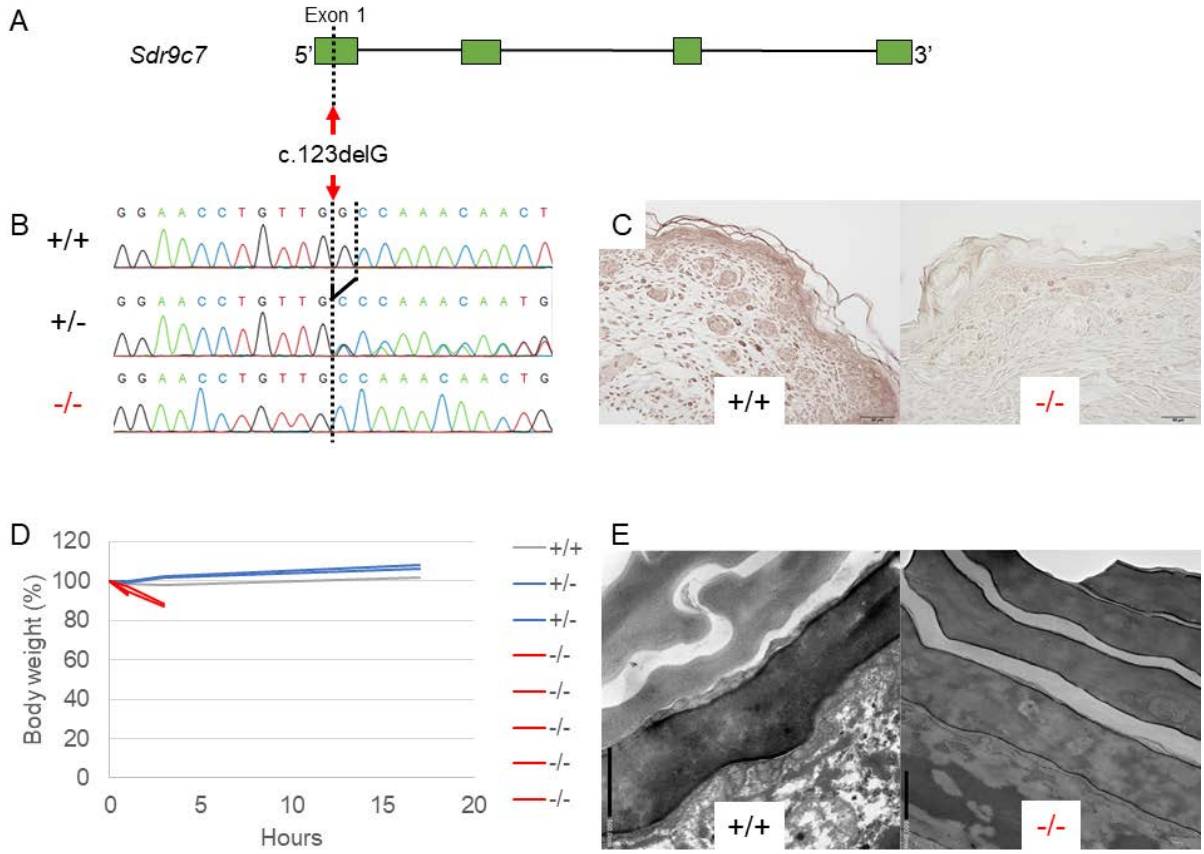


**Supplemental Figure 2. Pathological features of *Sdr9c7* knockout mice.**
(A) Schema of the *Sdr9c7* gene. Boxes indicate exons, and the dotted line indicates genomic mutation point. (B) Sequence data of *Sdr9c7* around the mutations in the *Sdr9c7*$^{+/+}$, *Sdr9c7*$^{+/-}$ and *Sdr9c7*$^{-/-}$ mice. Arrow indicates c.123delG. (C) Immunohistochemical staining for Sdr9c7 in skin sections from *Sdr9c7*$^{+/+}$ and *Sdr9c7*$^{-/-}$ newborns. Scale bars = 50 µm. (D) Monitoring of body weights of *Sdr9c7*$^{+/+}$, *Sdr9c7*$^{+/-}$ and *Sdr9c7*$^{-/-}$ mice after birth. (E) Transmission electron microscopy of the stratum corneum in *Sdr9c7*$^{+/+}$ and *Sdr9c7*$^{-/-}$ newborn mice (low magnification). Scale bars = 500 µm.

**Supplemental Figure 3.**

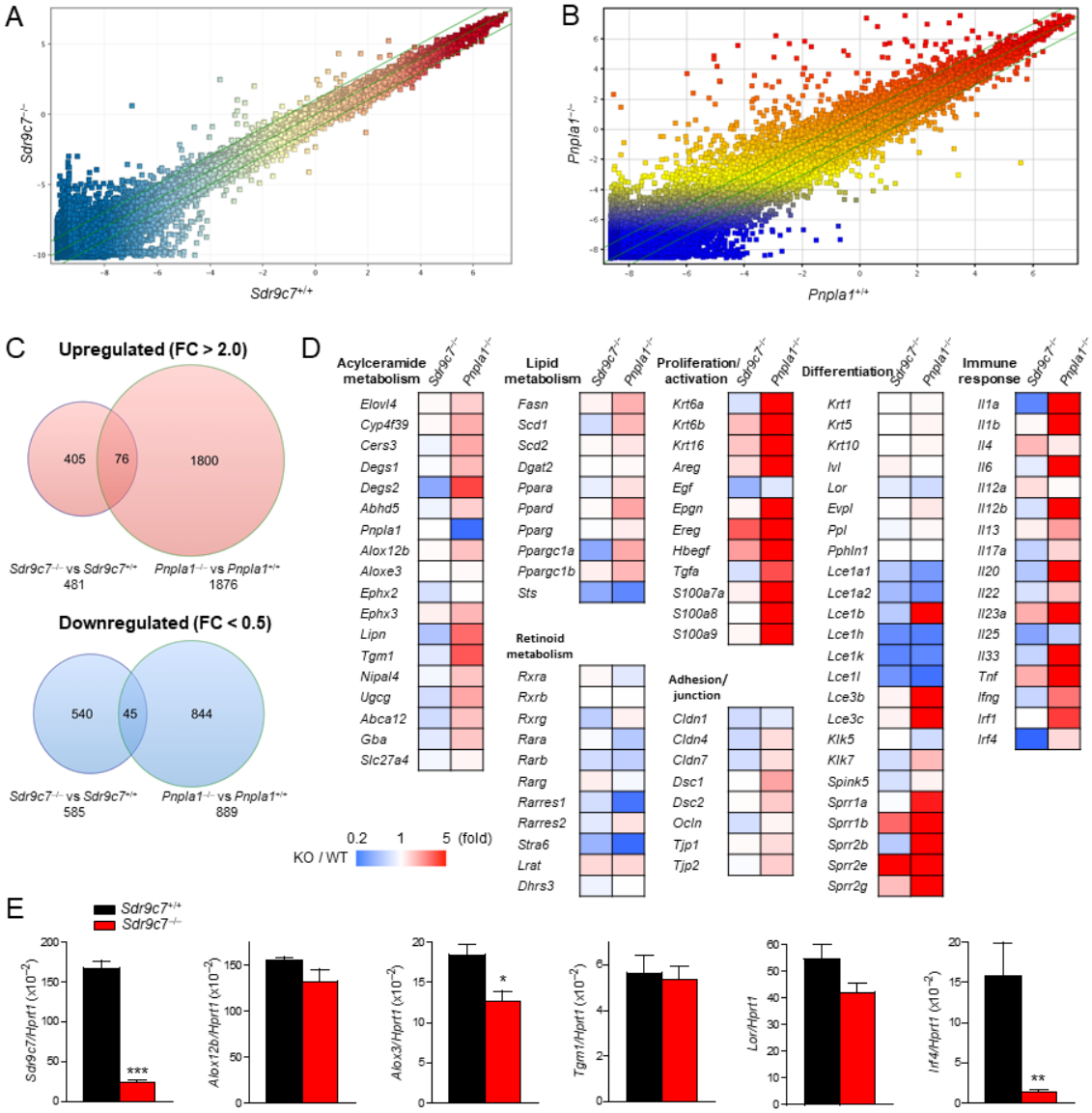


**Supplemental Figure 3. Gene expression analyses of *Sdr9c7* knock out mice.**

(A–D) Comparison of gene expression profiles in the neonatal skin between *Sdr9c7*$^{-/-}$ mice and *Pnpla1*$^{-/-}$ mice by DNA microarray analysis. (A and B) Scatter plots representing gene expression profiles of *Sdr9c7*$^{-/-}$ mice versus *Sdr9c7*$^{+/+}$ mice (A) and *Pnpla1*$^{-/-}$ mice versus *Pnpla1*$^{+/+}$ mice (B). (C) Venn diagram depicting the overlapping DEGs between *Sdr9c7*$^{-/-}$ skin and *Pnpla1*$^{-/-}$ skin. FC, fold change. (D) Heatmap showing fold change of representative genes associated with acylceramide metabolism, lipid metabolism, retinoid metabolism, keratinocyte proliferation/activation, adhesion/junction, keratinocyte differentiation, and immune response in *Sdr9c7*$^{-/-}$ skin and *Pnpla1*$^{-/-}$ skin (data in *Pnpla1*$^{-/-}$ skin were modified from Reference (3)). The color scale bar indicates the fold-change range of knockout mice relative to wild-type controls (KO/WT). The commonly upregulated genes (FC > 2.0) included those involved in keratinocyte proliferation linked to epidermal growth factor signaling (for example, *Ereg* and *Hbegf* ), CCE constituents such as small proline-rich region proteins (*Sprr1b*, *Sprr2e*, and *Sprr2g*), and skin-associated immune response (for example, *Il23a* and *Tnf*). The overlapping downregulated genes (FC <0.5) included late cornified envelope proteins

(*Lce1h*, *Lce1k*, and *Lce1l*). Regulatory diversification of SPRR and LCE within groups has been suggested to permit specific responsiveness to environmental challenge (14, 15). (E) Real-time PCR analysis showing mRNA expression levels of the selected genes in *Sdr9c7*$^{-/-}$ skin compared to *Sdr9c7*$^{+/+}$ skin. Data are expressed as the amount of mRNA normalized to endogenous *Hprt1* expression. Error bars represent the standard error of the mean (n = 4–5 animals per genotype). **P* < 0.05; ***P* < 0.01; and * *P* < 0.001, 2-tailed Student's *t* test.

**Supplemental Figures 4-15.**
**LC-MS analysis of mouse pup epidermal ceramides**

The following series of Supplementary Figures 4-15 illustrate results from LC-MS analysis of a MeOH/$CHCl_3$ extract of *Sdr9c7*$^{-/-}$ mouse neonate epidermis previously fractionated on an open-bed silica cartridge (discarding the initial hexane/ $CHCl_3$ (1:1, v/v) eluate and collecting the subsequent $CHCl_3$/10% MeOH fraction). Aliquots were run on a Phenomenex Luna 5μ silica column (25 x 0.2 cm) in normal phase mode with an initial solvent of hexane/isopropanol/glacial acetic acid (95:5:0.1, by volume) on a solvent gradient to the proportions 75:25:01 over 15 min (and held there until 20 min) at a flow rate of 0.6 ml/min. The column was interfaced with a Thermo LTQ linear ion trap triple-quad mass spectrometer recording under APCI conditions and scanning the mass range m/z 200 – 2000 in either positive ion or negative ion mode in different chromatographic runs. The main peaks in the wild-type and *Sdr9c7*$^{-/-}$ epidermis were essentially the same (see main text Figure 3) with the exception of the two extra peaks at 6.5 and 11.9 min in the *Sdr9c7* knockout epidermis.

**Supplemental Figure 4.**

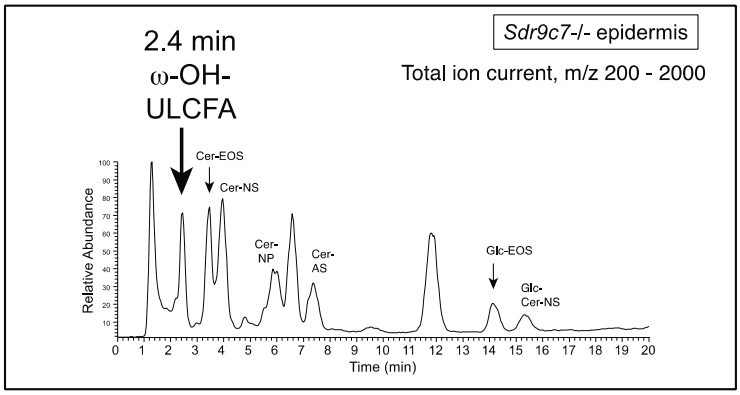


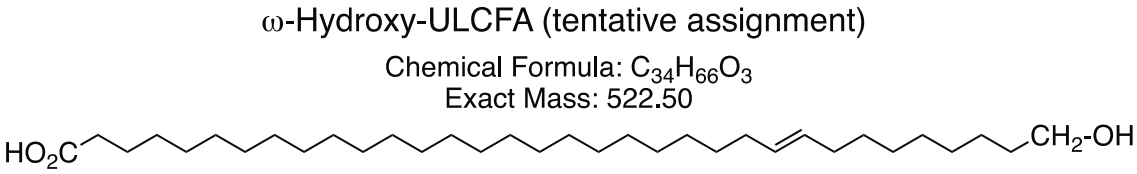


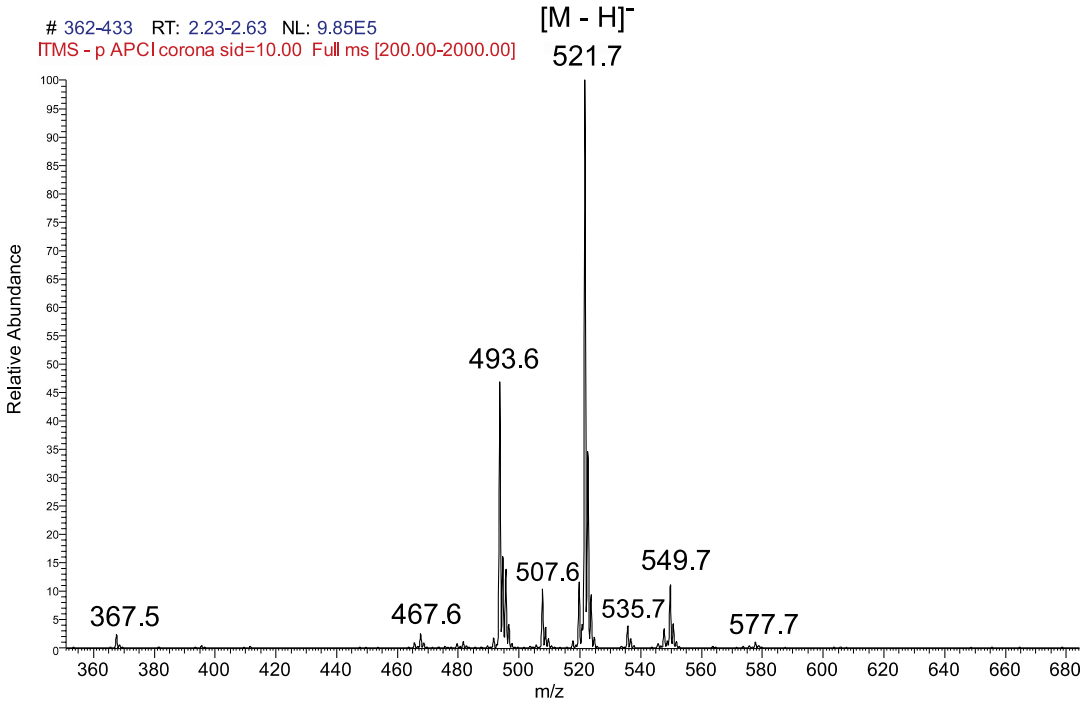


**Supplemental Figure 4. Negative ion APCI mass spectrum of the peak at 2.4 min (ω-OH-ULCFA) from the normal-phase LC-MS of epidermal lipids from *Sdr9c7*$^{-/-}$ epidermis.** The structural assignment is tentative and is based the appropriate elution time on LC-MS for a mono-hydroxy fatty acid and on the major ion at m/z 521.7 corresponding to [M – H]- for an ω-OH-(34:1)-ULCFA. The ions at m/z 549.7 and 493.6 represent the equivalent 36:1 and 32:1 ω-OH-ULCFA species.

**Supplemental Figure 5.**

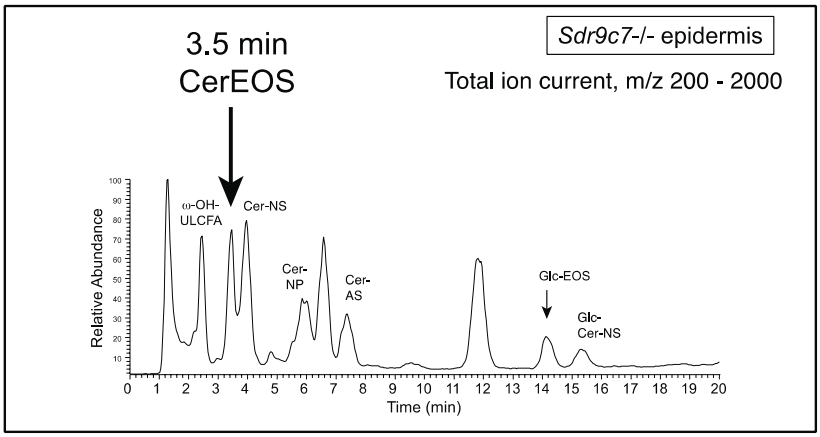


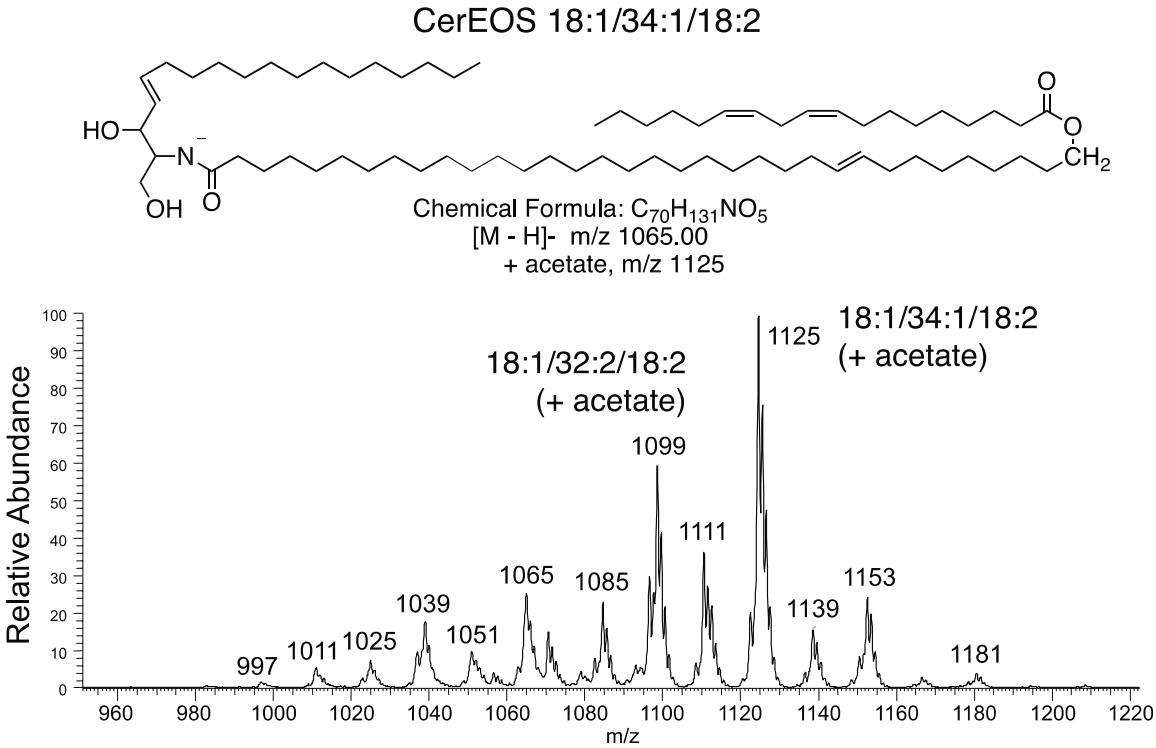


**Supplemental Figure 5. Negative ion APCI mass spectrum of the peak at 3.5 min (CerEOS) from the normal-phase LC-MS of epidermal lipids from *Sdr9c7*$^{-/-}$ epidermis.** The spectrum is CerEOS comprised of a mixture of differing chain lengths of the ω-OH-ULCFA, mainly the 18:1/34:1/18:2 species (m/z 1065 and its acetate adduct ion m/z 1125).

**Supplemental Figure 6.**

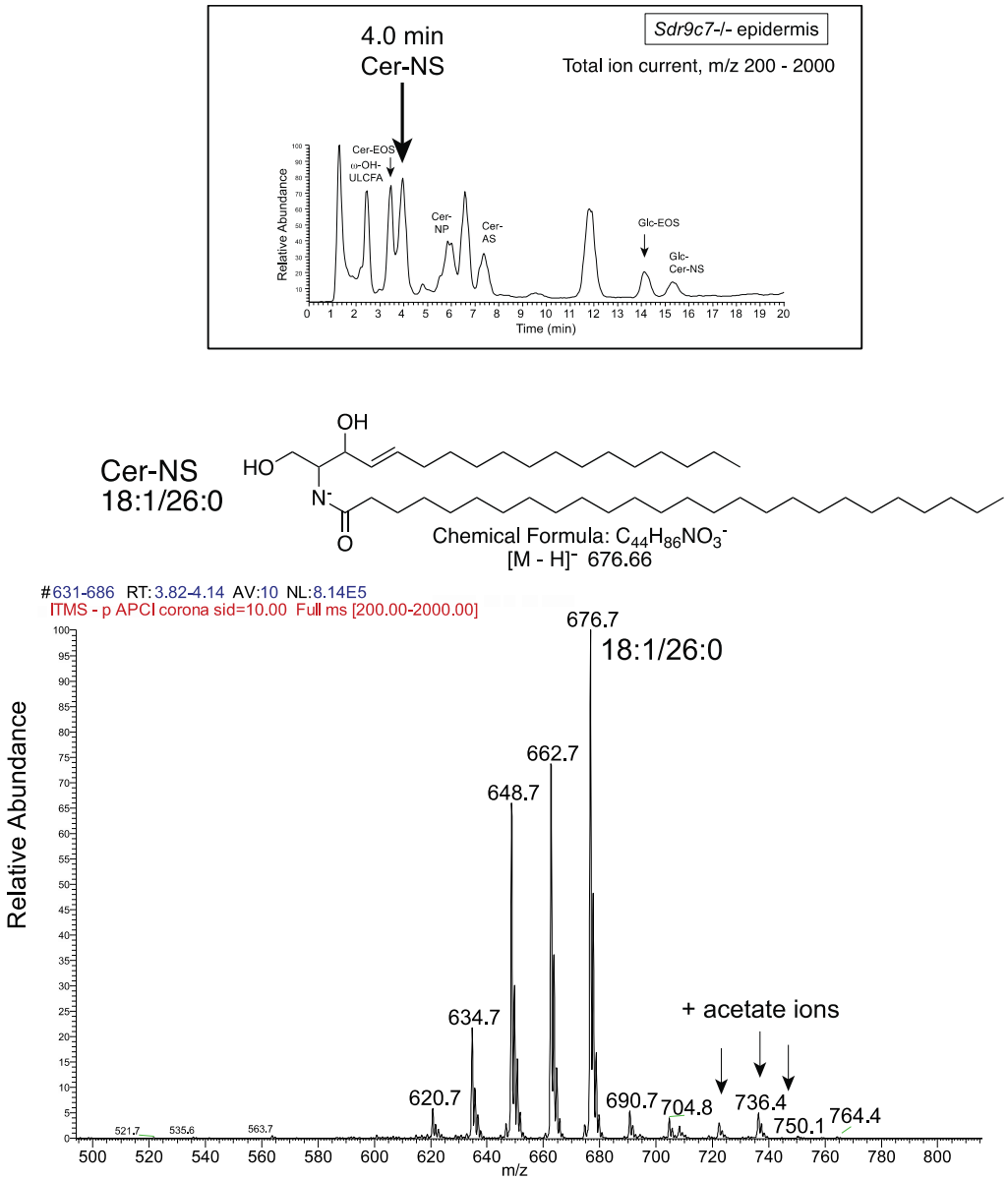


**Supplemental Figure 6. Negative ion APCI mass spectrum of the peak at 4.0 min (CerNS) from the normal-phase LC-MS of epidermal lipids from *Sdr9c7*$^{-/-}$ epidermis.**

The polarity on LC-MS and the mass spectrum identify the peak as Cer-NS. The most prominent ion, m/z 676.7, corresponds to CerNS 18:1/26:0, the other ions showing gain or loss of increments of $CH_2$ (14 a.m.u.). Arrows point to the corresponding acetate adduct ions.

**Supplemental Figure 7.**

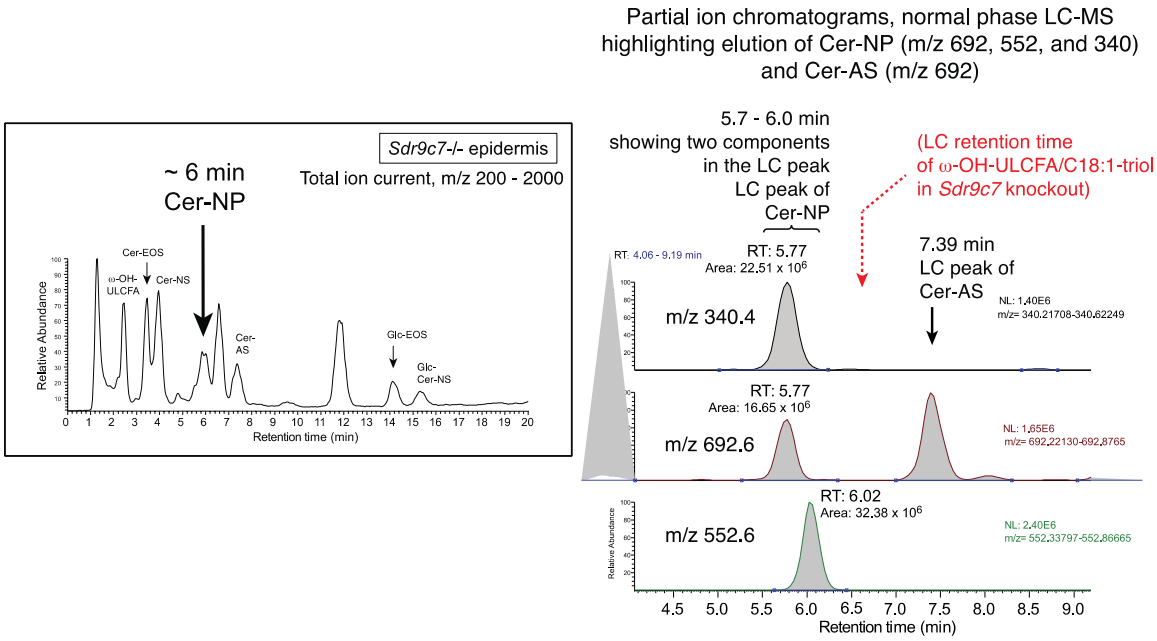


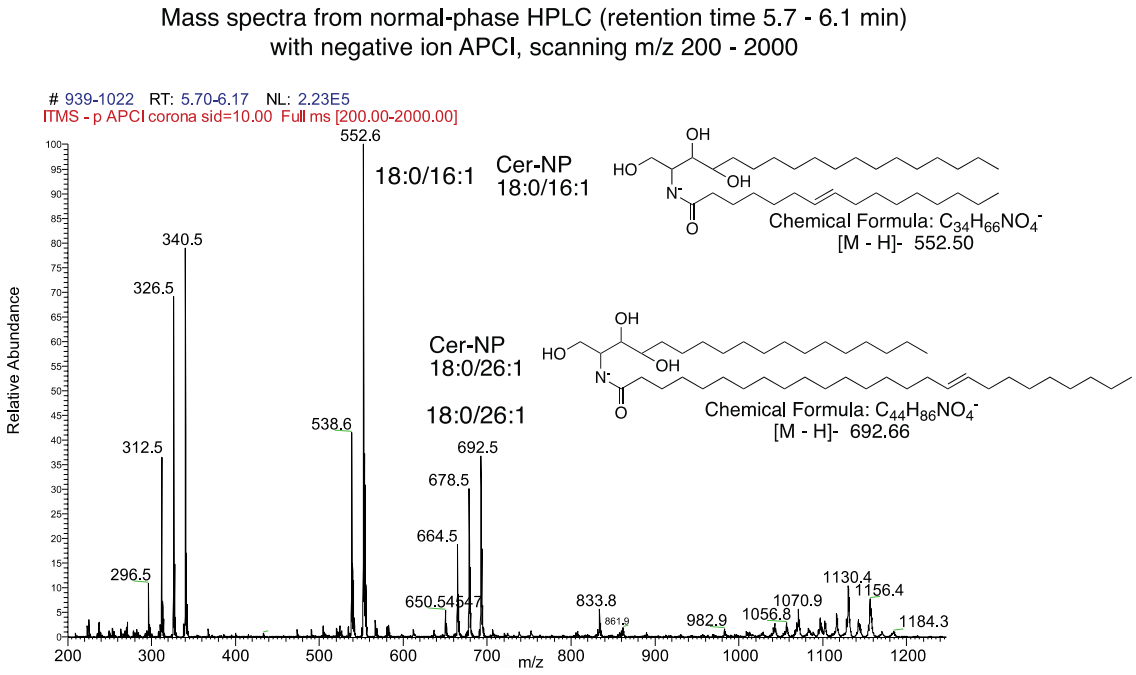


**Supplemental Figure 7. Negative ion APCI mass spectrum of the peak at ~6 min (CerNP) from the normal-phase LC-MS of epidermal lipids from *Sdr9c7*$^{-/-}$ epidermis.**

The structural assignment is compatible with the polarity of CerNP on normal-phase LC-MS (16, 17) and m/z values of the major ions. The spectrum shows a mixture of CerNP

components that separate very slightly on LC and are identified as CerNP(18:0/16:1) and CerNP(18:0/26:1). The partial ion chromatograms (top right) show the precise co-elution of m/z 340.5 with m/z 692.5 at 5.77 min, suggesting the lower mass ion arises from in-source fragmentation of m/z 692.5, the latter representing Cer-NP 18:0/26:1. The very slightly later-eluting component at 6.02 min is detected at m/z 552.6 and is assigned as CerNP (18:0/16:1). The second peak of m/z 692.5 eluting at 7.39 min in the partial ion chromatogram represents CerAS(18:1/26:0), a ceramide with the same molecular weight at CerNP and significantly more polar elution on LC-MS (16, 17). Finally, the very high molecular mass ions at m/z values of 1130.4 and 1156.4 may represent the acetate adduct ions of CerEOS-epoxyalcohol with ω-OH-ULCFA components of 32:0 and 34:1 respectively; this product accumulates in the *Sdr9c7*$^{-/-}$ epidermis and is in far lower abundance in the wild-type.

**Supplemental Figure 8.**

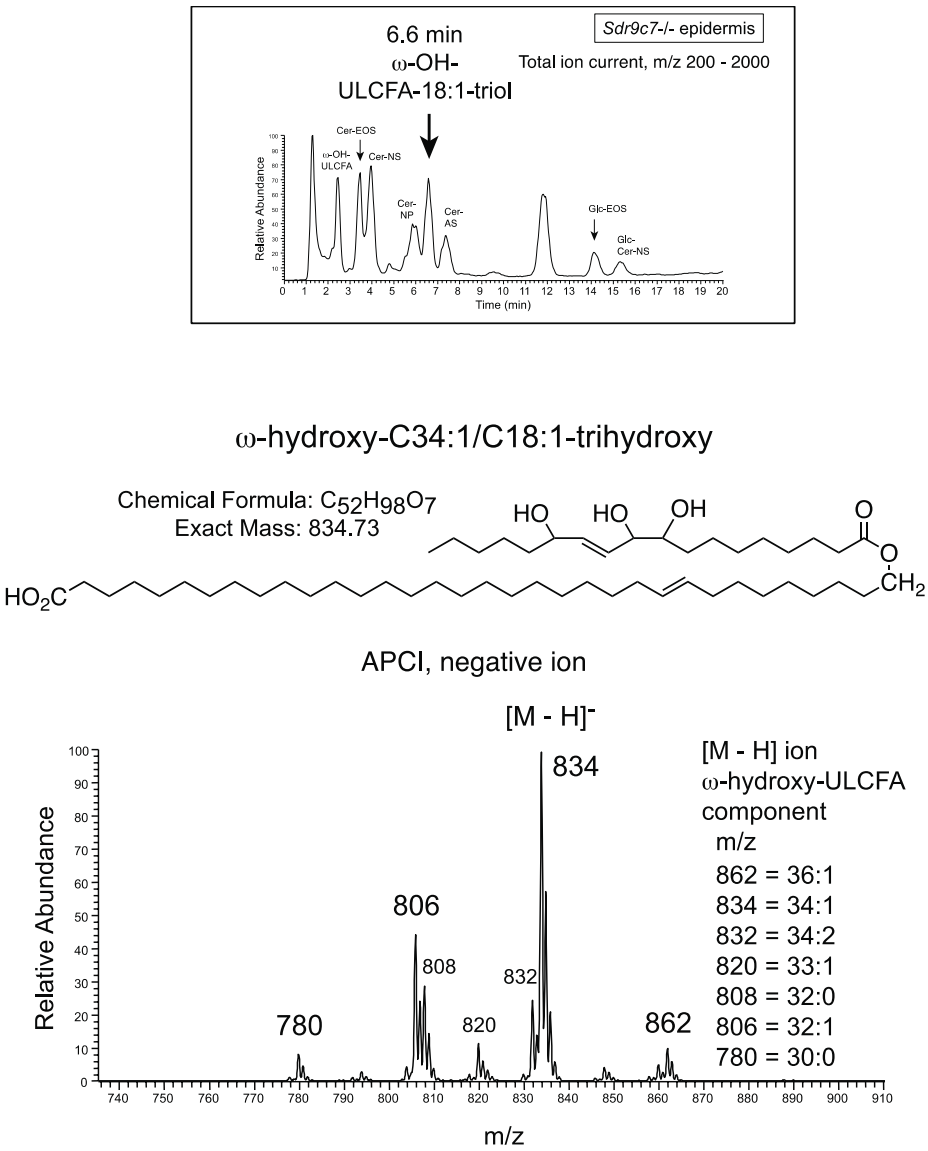


**Supplemental Figure 8. Negative ion APCI mass spectrum of the peak at 6.6 min (ω-OH-ULCFA/C18:1-triol) from the normal-phase LC-MS of epidermal lipids from *Sdr9c7*$^{-/-}$ epidermis.**

The polarity on LC-MS and the most prominent ion in the mass spectrum at m/z 834 identify the main component as 34:1 ω-OH-ULCFA esterified with C18:1-triol. Other species of the ω-OH-ULCFA component are represented by ions at m/z 862 (36:1), m/z 820 (33:1), m/z 808 (32:0), m/z 806 (32:1), and m/z 780 (30:0). Evidence of the two main components is provided in the next figure in this series.

**Supplemental Figure 9.**

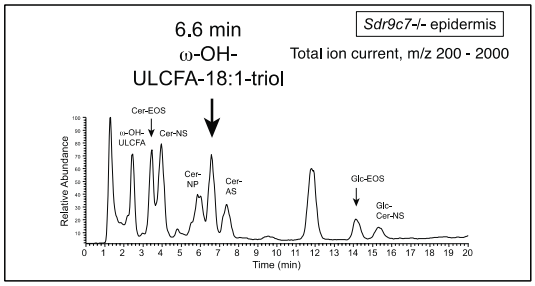


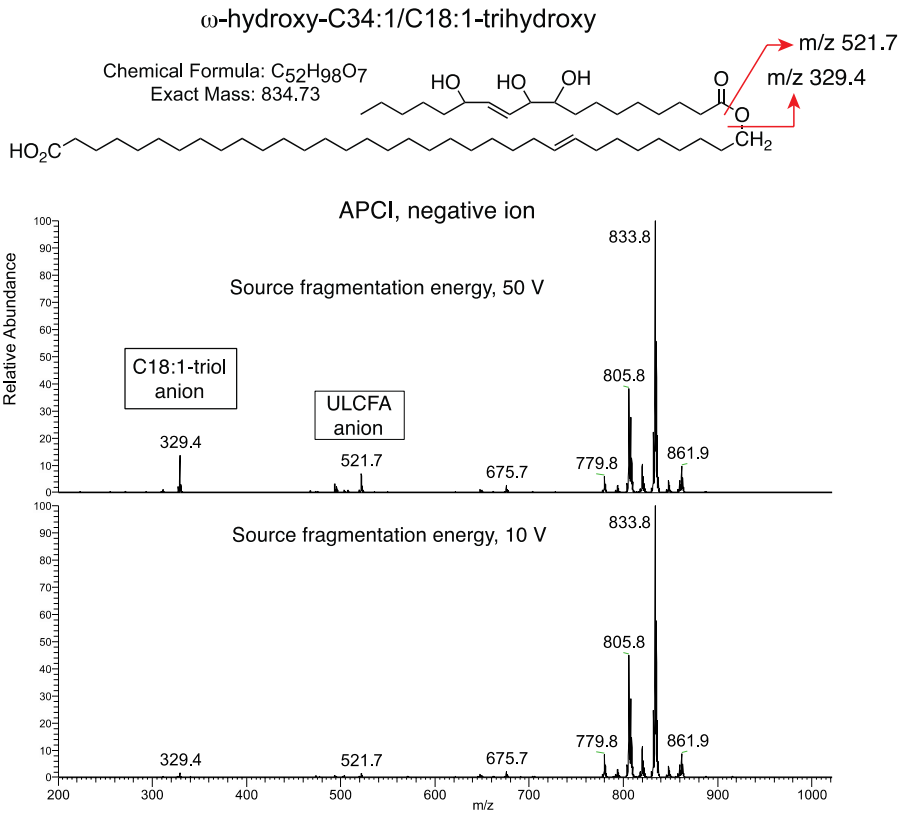


**Supplemental Figure 9. Negative ion APCI mass spectrum of the peak at 6.6 min with in-source fragmentation confirming identification of ω-OH-ULCFA/C18:1 triol.**

Fragment ions of major structural significance arising from m/z 833.8 (834, $[M - H]^-$) are m/z 521.7, corresponding to the 34:1 ω-OH-ULCFA component and m/z 329.4 representing the C18:1-triol. These appear more prominently in the upper spectrum in which the CID voltage is increased from 10 V to 50 V.

**Supplemental Figure 10.**

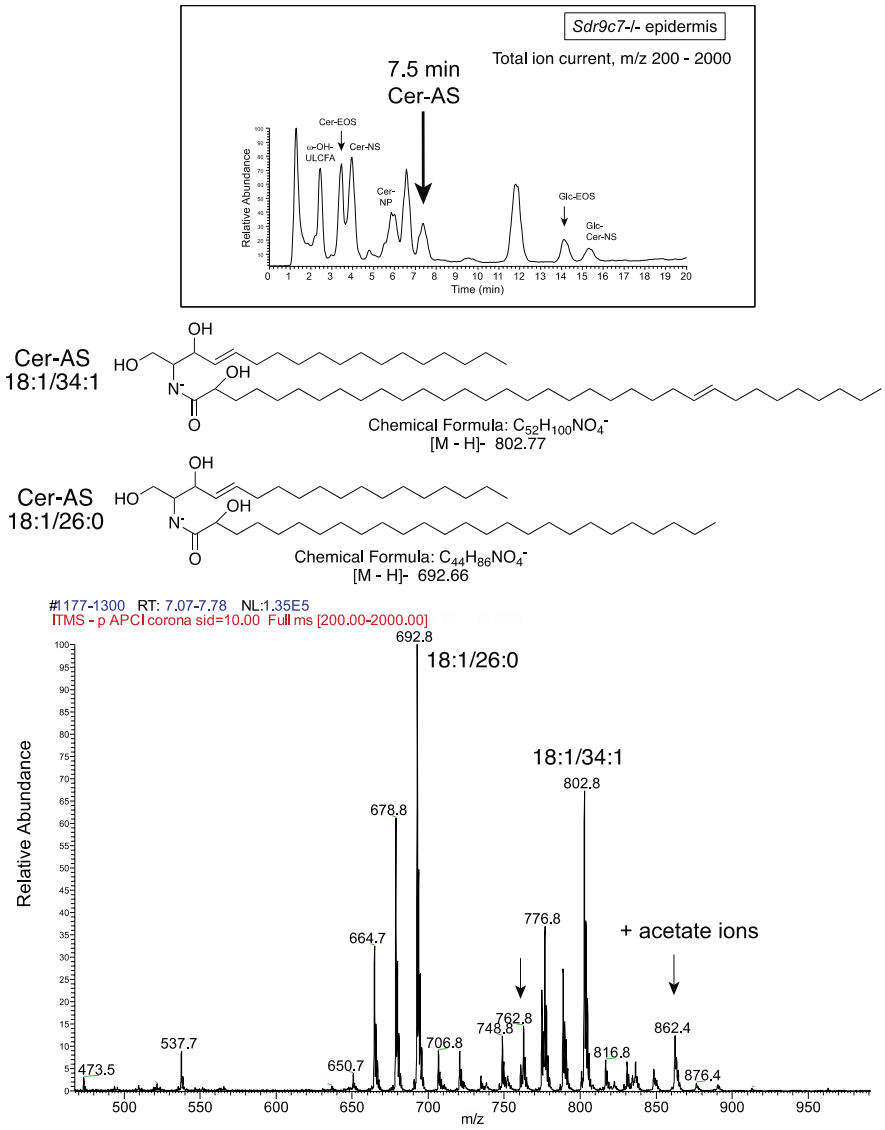


**Supplemental Figure 10. Negative ion APCI mass spectrum of the peak at 7.5 min (Cer-AS) from the normal-phase LC-MS of epidermal lipids from *Sdr9c7*$^{-/-}$ epidermis.**

The polarity on LC-MS (16, 17) and the most prominent ions in the mass spectrum identify the peak as CerAS. Similar to CerNP, the CerAS LC peak is a mixture of two main components, in this case identified as 18:1/26:0 (m/z 692.8) and 18:1/34:1 (m/z 802.8). The arrows indicate the acetate ion adducts from m/z 692.8 and m/z 802.8.

**Supplemental Figure 11.**

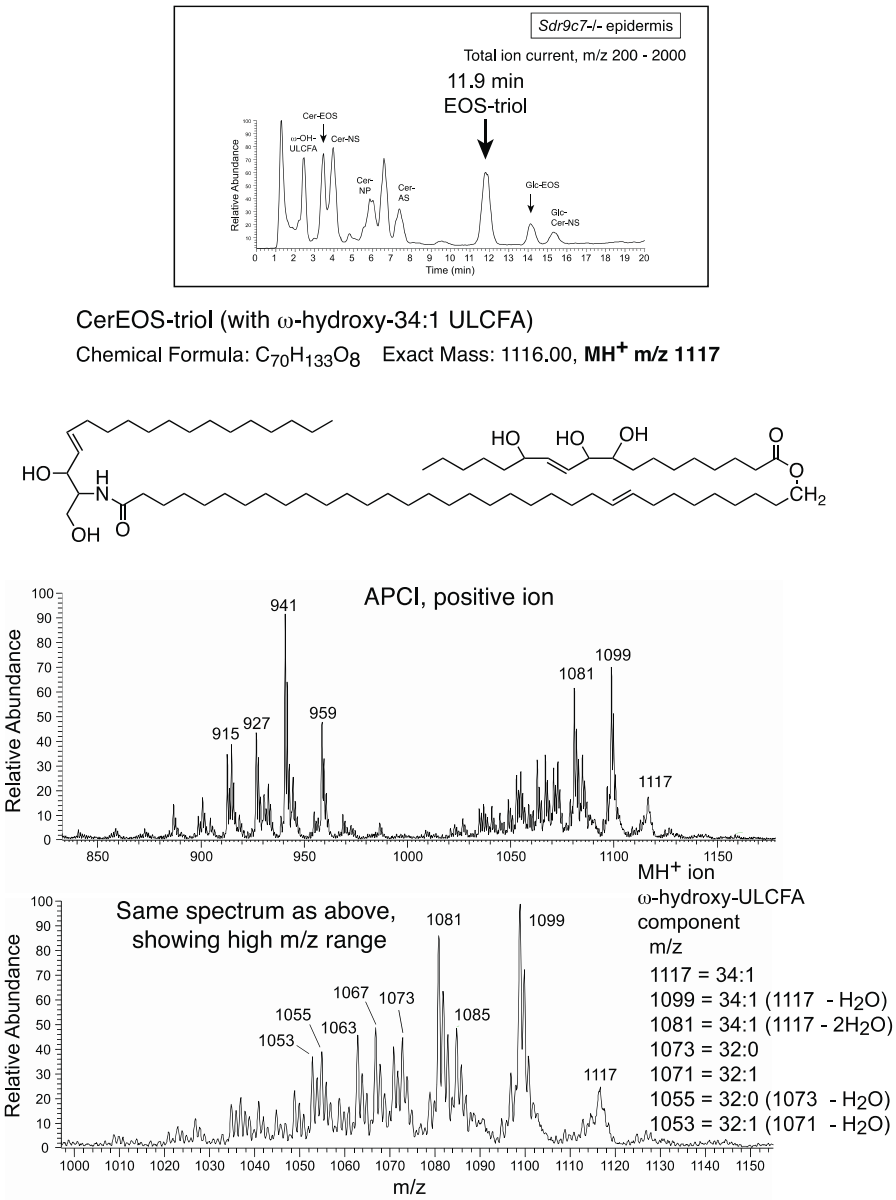


**Supplemental Figure 11. Positive ion APCI mass spectrum of the peak at 11.9 min (CerEOS-triol) from the normal-phase LC-MS of epidermal lipids from *Sdr9c7*$^{-/-}$ epidermis.**

The main species has a $MH^+$ ion at m/z 1117 with a prominent [$MH^+$ – $H_2O$] ion at m/z 1099, and [$MH^+$ – $2H_2O$] at m/z 1081, each attributable to CerEOS containing a C34:1 ω-hydroxy-ULCFA esterified with a fatty acid C18:1-triol. Further support for the structure is provided in the following two Supplemental figures.

**Supplemental Figure 12.**

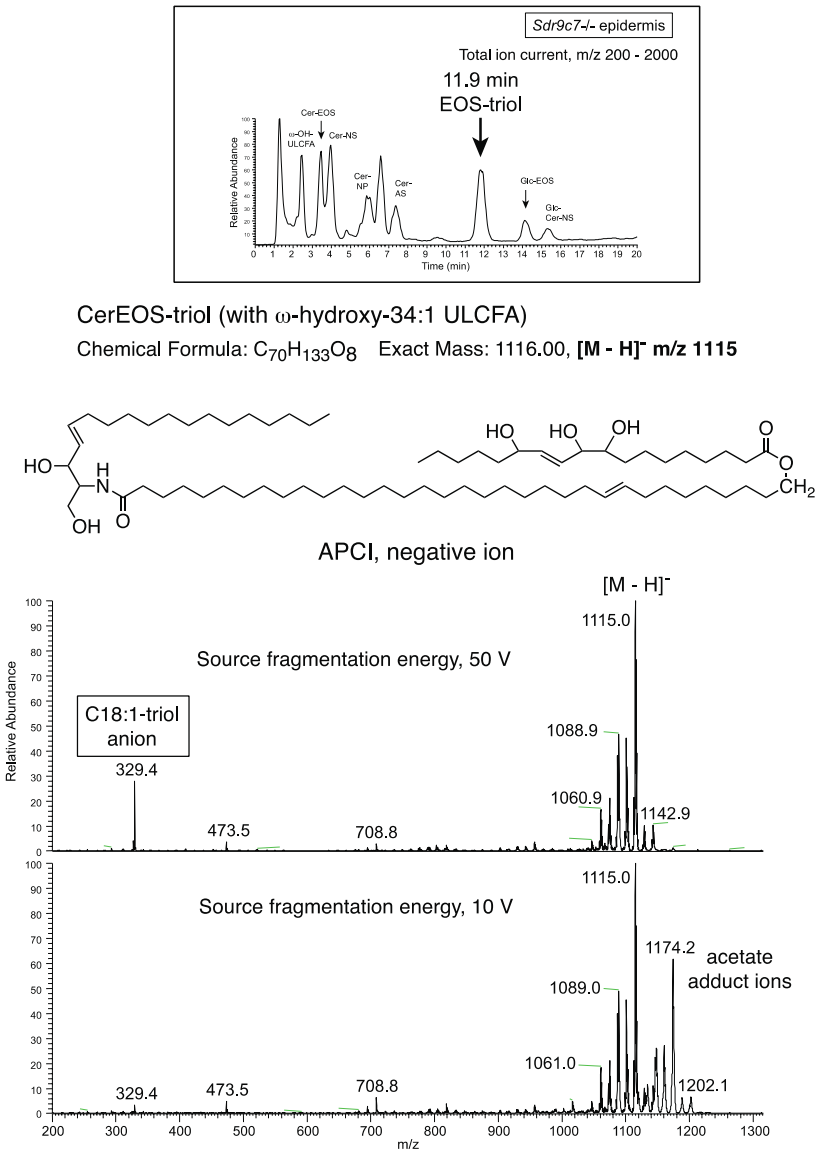


**Supplemental Figure 12. Negative ion APCI mass spectra of the peak at 11.9 min (CerEOS-triol) with in-source fragmentation identifying the C18:1-triol component.**

The lower of the two mass spectra was recorded with a relatively low source fragmentation energy of 10 V, producing the $[M - H]^-$ and also resulting in m/z 1174.2 and other acetate adduct ions, (acetate coming from the HPLC solvent). At higher source voltage the acetate adduct ions disappear and a more prominent ion at m/z 329 represents the C18:1-triol component of the molecule.

**Supplemental Figure 13.**

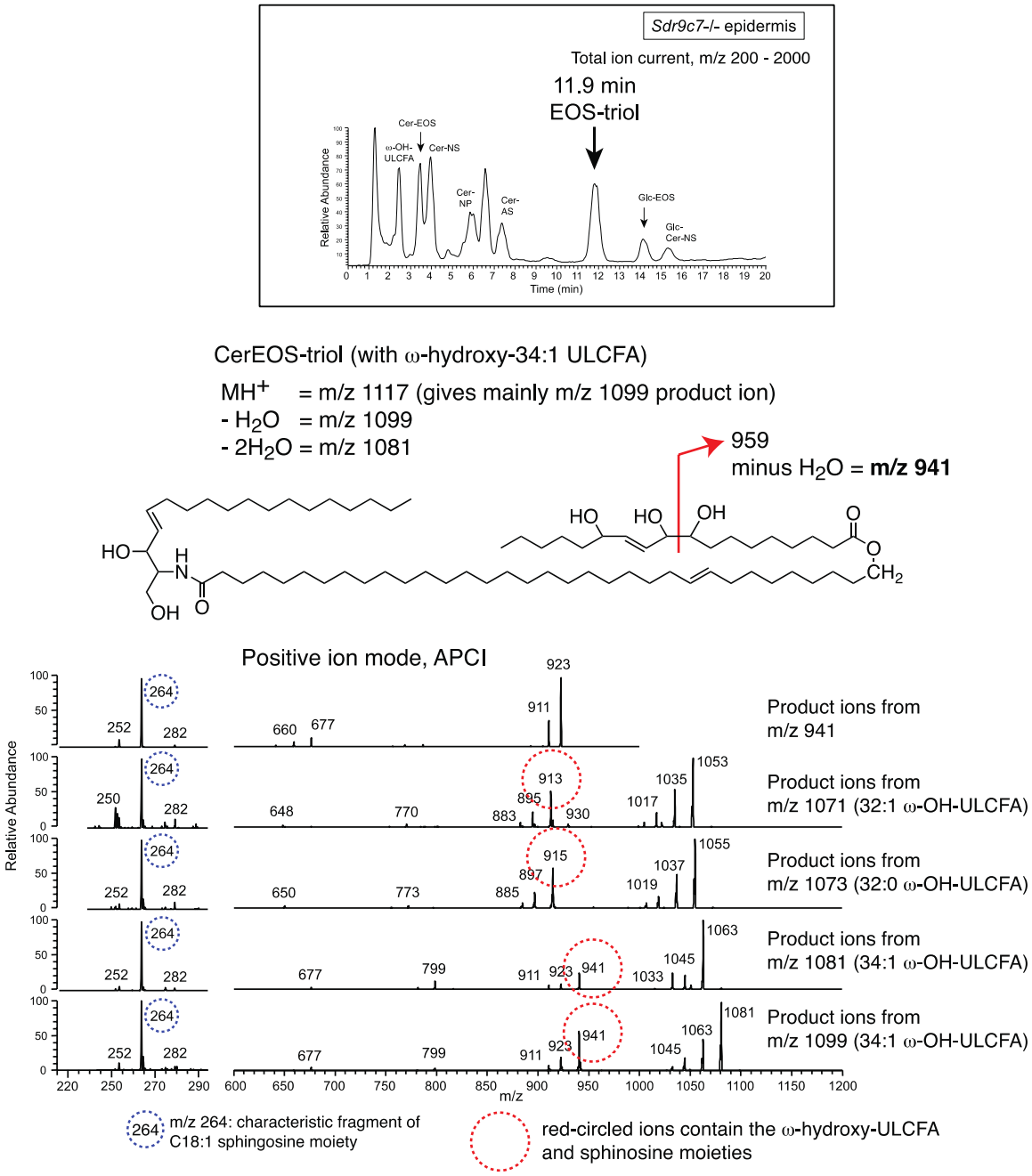


**Supplemental Figure 13. Positive APCI product ion mass spectra of the peak at 11.9 min (CerEOS-triol) with in-source fragmentation of the major ions.**

Product ions were generated from the major ions in the positive ion APCI spectrum (Figure 11). The $MH^+$ ion at m/z 1117, representing CerEOS-triol (18:1/34:1/18:1-triol), produced mainly m/z 1099 from loss of water (not shown). The product ion spectra are,

from the bottom upwards, from m/z 1099 ([MH – $H_2O$]+ with 34:1 ω-OH-ULCFA), m/z 1081 ([MH – $2H_2O$]+ with 34:1 ω-OH-ULCFA), m/z 1073 (with 32:0 ω-OH-ULCFA), and m/z 1071 (with 32:1 ω-OH-ULCFA). The product ion spectrum on top is from m/z 941 (itself a prominent product ion from m/z 1099 and 1081). The m/z 941 product ion from the 34:1 containing CerEOS-triol shifts to m/z 915 and 913 from m/z 1073 and 1071 respectively, indicating its retention of the ω-OH-ULCFA. Based on these observations, the chemical structure shows a likely origin of the m/z 941 product ion. The lower mass range in each product ion spectrum shows ions at m/z 282, most prominently at m/z 264, and m/z 252. This group of ions is characteristically formed from a C18:1 sphingosine moiety (e.g. refs (18-21)), and thus defines this component of the CerEOS-triol structure.

**Supplemental Figure 14.**

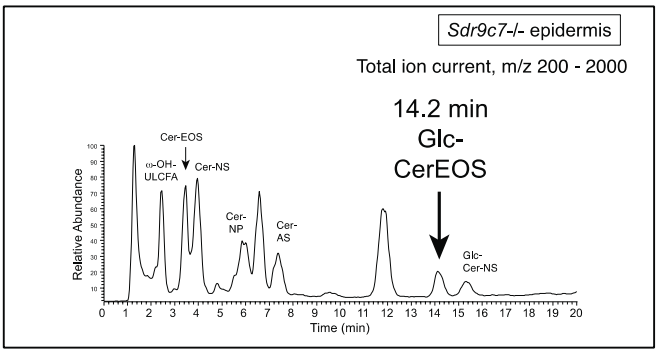


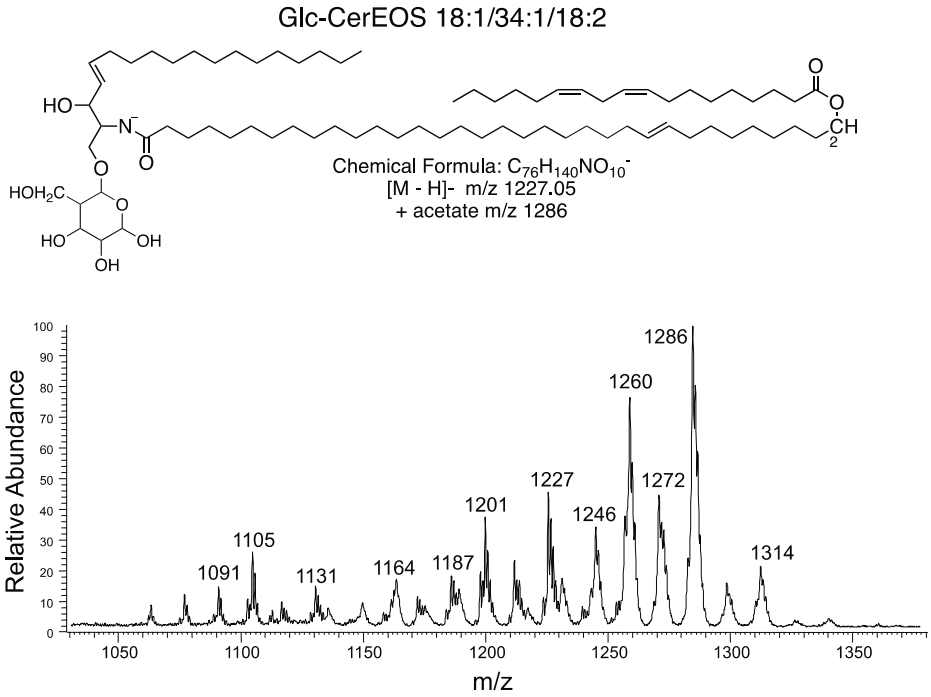


**Supplemental Figure 14. Negative ion APCI mass spectrum of the peak at 14.2 min (Glc-CerEOS) from the normal-phase LC-MS of epidermal lipids from *Sdr9c7*$^{-/-}$ epidermis.**

The spectrum identifies Glc-CerEOS of differing chain lengths of the ω-OH-ULCFA, mainly the 18:1/34:1/18:2 species. The major ion at m/z 1286 represents the acetate adduct ion of the $[M – H]^-$ ion at m/z 1227 containing 34:1 ω-OH-ULCFA.

**Supplemental Figure 15.**

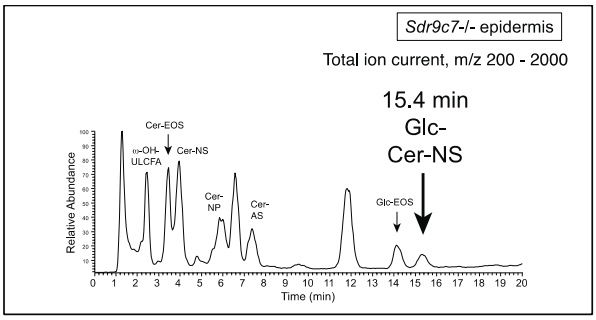


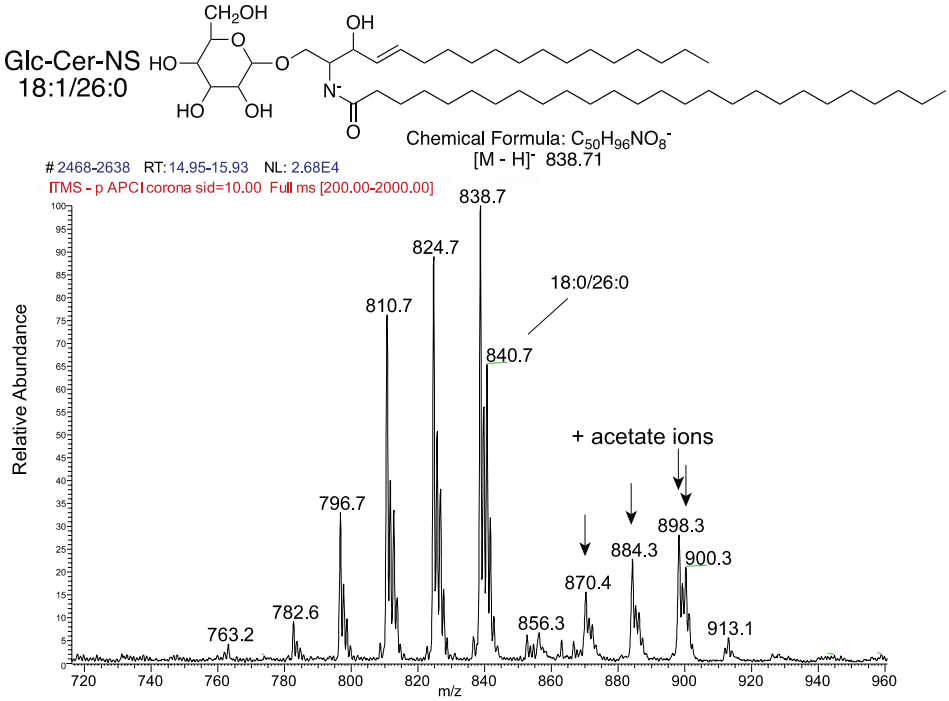


**Supplemental Figure 15. Negative ion APCI mass spectrum of the peak at 15.4 min (Glc-CerNS) from the normal-phase LC-MS of epidermal lipids from *Sdr9c7*$^{-/-}$ epidermis.**

The base peak at m/z 838.7 represents the $[M – H]^-$ ion of Glc-CerNS containing a 18:1 sphingosine moiety and 26:0 ULCFA. Other $[M – H]^-$ ions differ by 14 a.m.u. and represent ULCFA components with differing carbon chain length. Arrows highlight the corresponding acetate adduct ions.

**Supplemental Figure 16.**

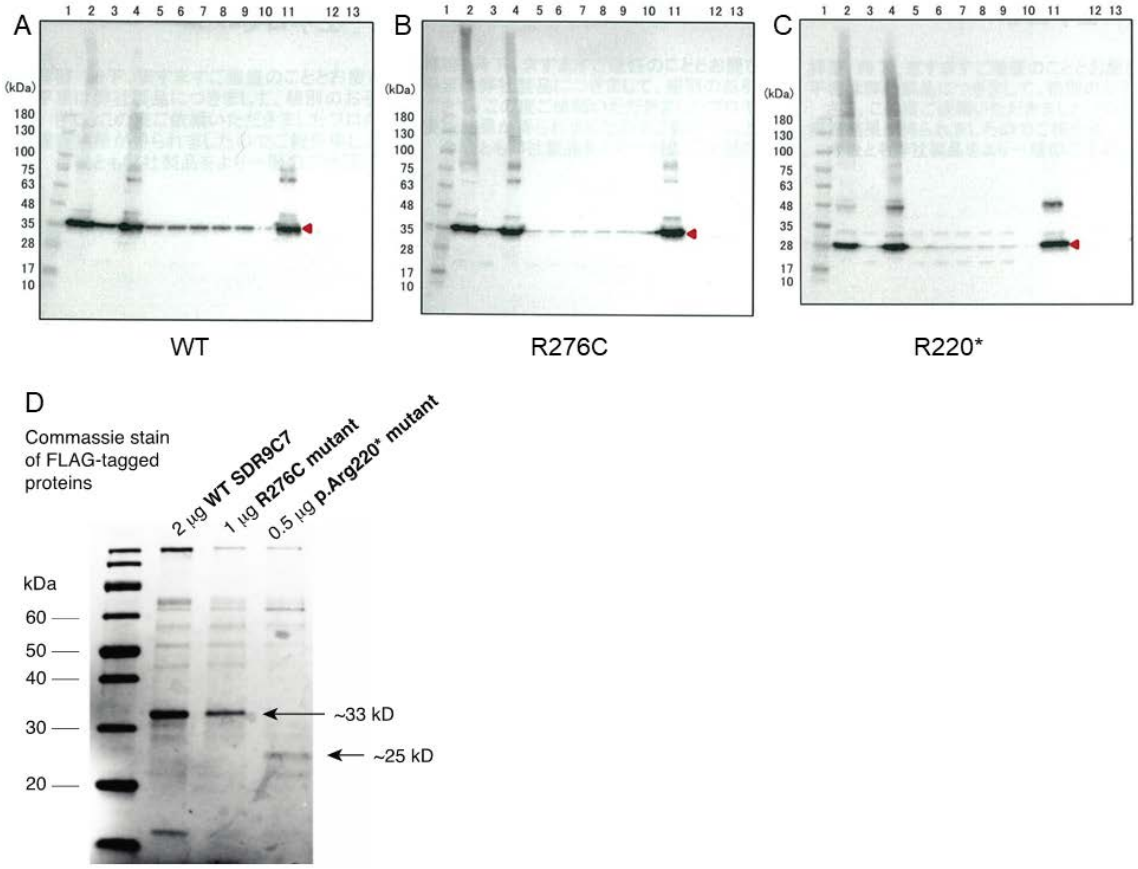


**Supplemental Figure 16. SDS-PAGE analysis of recombinant human SDR9C7 proteins.**

(A-C) Western blots of recombinant SDR9C7 using anti-FLAG M2-peroxidase (HRP); (A) wild type, (B) R276C, (C) R220*. Red arrows identify the SDR9C7 proteins. (D) Commassie stained gels of wild-type, R276C mutant and R220* mutant.

## Supplemental Tables

**Supplemental Table 1. Amounts of total ceramide and each ceramide class in the stratum corneum of the upper arm from the patient and her parents: comparison with those of normal controls.**

| Ceramide level (ng/μg protein) | Patient (p.Arg276Cys homo) | Father (p.Arg276Cys hetero) | Mother (p.Arg276Cys hetero) | Controls, n=8 (mean±SD) |
|---|---|---|---|---|
| NDS | 1.75 | 1.70 | 1.88 | 1.40±0.26 |
| NS | 3.46 | 1.94 | 2.03 | 1.80±0.36 |
| NH | 3.19 | 4.36 | 3.35 | 3.67±0.67 |
| NP | 2.98 | 5.02 | 3.37 | 4.94±0.78 |
| ADS | 0.51 | 0.32 | 0.46 | 0.33±0.11 |
| AS | 2.84 | 0.95 | 1.28 | 1.31±0.42 |
| AH | 2.59 | 2.10 | 2.07 | 2.42±0.41 |
| AP | 1.57 | 1.75 | 1.29 | 2.15±0.32 |
| EOS | 6.81 | 2.75 | 1.66 | 2.40±0.45 |
| EOH | 0.19 | 1.15 | 0.70 | 1.22±0.43 |
| EOP | 0.12 | 0.33 | 0.15 | 0.29±0.10 |
| Total | 26.01 | 22.39 | 18.24 | 21.93±3.03 |

Abbreviations: SD, standard deviation

**Supplemental Table 2. Amounts of total ceramide and each ceramide class in the stratum corneum of the forearm from the patient and her parents: comparison with those of normal controls.**

| Ceramide level (ng/μg protein) | Patient (p.Arg276Cys homo) | Father (p.Arg276Cys hetero) | Mother (p.Arg276Cys hetero) | Controls, n=8 (mean±SD) |
|---|---|---|---|---|
| NDS | 1.46 | 1.93 | 1.96 | 1.44±0.31 |
| NS | 2.40 | 1.76 | 2.94 | 1.91±0.46 |
| NH | 2.50 | 4.26 | 4.25 | 3.43±0.38 |
| NP | 2.39 | 4.81 | 3.51 | 4.59±0.67 |
| ADS | 0.32 | 0.36 | 0.43 | 0.33±0.08 |
| AS | 1.57 | 0.86 | 1.76 | 1.14±0.37 |
| AH | 1.67 | 1.89 | 2.59 | 1.98±0.42 |
| AP | 1.17 | 1.59 | 1.32 | 1.63±0.33 |
| EOS | 4.86 | 2.20 | 2.17 | 2.40±0.55 |
| EOH | 0.38 | 1.04 | 1.07 | 0.88±0.39 |
| EOP | 0.08 | 0.40 | 0.17 | 0.33±0.08 |
| Total | 18.80 | 21.12 | 22.18 | 20.05±2.91 |

Abbreviations: SD, standard deviation

**Supplemental Table 3. Persentages of ceramide composition in the stratum corneum of the upper arm from the patient and her parents: comparison with those of normal controls.**

| Ceramide composition (%) | Patient (p.Arg276Cys homo) | Father (p.Arg276Cys hetero) | Mother (p.Arg276Cys hetero) | Controls, n=8 (mean±SD) |
|---|---|---|---|---|
| NDS | 6.74 | 7.59 | 10.29 | 6.42±0.98 |
| NS | 13.30 | 8.68 | 11.12 | 8.17±0.81 |
| NH | 12.25 | 19.50 | 18.36 | 16.73±2.01 |
| NP | 11.46 | 22.45 | 18.47 | 22.56±2.22 |
| ADS | 1.96 | 1.45 | 2.53 | 1.54±0.54 |
| AS | 10.90 | 4.27 | 7.04 | 5.93±1.52 |
| AH | 9.97 | 9.37 | 11.36 | 11.05±1.05 |
| AP | 6.04 | 7.83 | 7.07 | 9.90±1.61 |
| EOS | 26.19 | 12.28 | 9.10 | 10.96±1.52 |
| EOH | 0.74 | 5.14 | 3.85 | 5.43±1.54 |
| EOP | 0.44 | 1.45 | 0.80 | 1.30±0.32 |
| Total | 100.00 | 100.00 | 100.00 | 100.00 |

Abbreviations: SD, standard deviation

**Supplemental Table 4. Persentages of ceramide composition in the stratum corneum of the forearm from the patient and her parents: comparison with those of normal controls.**

| Ceramide composition (%) | Patient (p.Arg276Cys homo) | Father (p.Arg276Cys hetero) | Mother (p.Arg276Cys hetero) | Controls, n=8 (mean±SD) |
|---|---|---|---|---|
| NDS | 7.76 | 9.16 | 8.85 | 7.13±0.70 |
| NS | 12.77 | 8.34 | 13.24 | 9.46±1.05 |
| NH | 13.29 | 20.19 | 19.14 | 17.20±1.29 |
| NP | 12.73 | 22.79 | 15.84 | 22.98±2.50 |
| ADS | 1.70 | 1.70 | 1.92 | 1.61±0.22 |
| AS | 8.34 | 4.08 | 7.93 | 5.63±1.24 |
| AH | 8.91 | 8.96 | 11.69 | 9.85±0.89 |
| AP | 6.24 | 7.52 | 5.97 | 8.15±1.18 |
| EOS | 25.83 | 10.43 | 9.80 | 11.94±1.87 |
| EOH | 2.01 | 4.94 | 4.84 | 4.38±1.88 |
| EOP | 0.42 | 1.90 | 0.78 | 1.67±0.53 |
| Total | 100.00 | 100.00 | 100.00 | 100.00 |

Abbreviations: SD, standard deviation

**Supplemental Table 5. Average carbon numbers of ceramide in the stratum corneum of the upper arm from the patient and her parents: comparison with those of normal controls.**

| Average carbon numbers of ceramide (caluculated by mol ratio) | Patient (p.Arg276Cys homo) | Father (p.Arg276Cys hetero) | Mother (p.Arg276Cys hetero) | Controls, n=8 (mean±SD) |
|---|---|---|---|---|
| NDS | 44.09 | 45.55 | 45.00 | 44.96±0.45 |
| NS | 44.33 | 44.75 | 43.91 | 44.60±0.41 |
| NH | 43.50 | 44.09 | 43.74 | 44.33±0.27 |
| NP | 44.58 | 44.56 | 44.31 | 44.56±0.22 |
| ADS | 41.37 | 41.61 | 39.78 | 41.34±0.41 |
| AS | 41.96 | 41.27 | 41.98 | 41.75±0.44 |
| AH | 43.12 | 43.29 | 43.17 | 43.41±0.21 |
| AP | 43.37 | 43.15 | 42.82 | 43.21±0.24 |
| EOS | 68.19 | 68.18 | 68.19 | 68.13±0.15 |
| EOH | 68.99 | 67.21 | 67.73 | 67.36±0.16 |
| EOP | 68.63 | 68.75 | 68.60 | 68.15±0.50 |

Abbreviations: SD, standard deviation

**Supplemental Table 6. Average carbon numbers of ceramide in the stratum corneum of the forearm from the patient and her parents: comparison with those of normal controls.**

| Average carbon numbers of ceramide (caluculated by mol ratio) | Patient (p.Arg276Cys homo) | Father (p.Arg276Cys hetero) | Mother (p.Arg276Cys hetero) | Controls, n=8 (mean±SD) |
|---|---|---|---|---|
| NDS | 45.24 | 45.78 | 45.06 | 44.96±0.63 |
| NS | 44.21 | 44.99 | 45.12 | 44.78±0.52 |
| NH | 43.81 | 44.21 | 44.17 | 44.10±0.33 |
| NP | 45.22 | 44.57 | 44.68 | 44.61±0.33 |
| ADS | 41.74 | 41.17 | 39.54 | 40.72±0.63 |
| AS | 41.81 | 42.30 | 41.73 | 41.74±0.44 |
| AH | 43.06 | 43.03 | 43.35 | 43.26±0.26 |
| AP | 43.99 | 43.34 | 43.01 | 43.24±0.34 |
| EOS | 68.29 | 68.42 | 67.94 | 68.35±0.25 |
| EOH | 66.85 | 67.38 | 67.32 | 67.88±0.50 |
| EOP | 68.77 | 68.25 | 68.10 | 68.22±0.49 |

Abbreviations: SD, standard deviation

**Supplemental Table 7. Amounts of total free fatty acids, cholesterol and ChSO4 in the stratum corneum of the upper arm from the patient and her parents: comparison with those of normal controls.**

| Total (ng/μg protein) | Patient (p.Arg276Cys homo) | Father (p.Arg276Cys hetero) | Mother (p.Arg276Cys hetero) | Controls, n=8 (mean±SD) |
|---|---|---|---|---|
| FFAs | 18.61 | 11.26 | 19.06 | 13.28±1.56 |
| Cholesterol | 24.96 | 16.26 | 23.75 | 11.31±3.30 |
| $ChSO_4$ | 1.33 | 0.85 | 0.73 | 0.92±0.22 |

Abbreviations: FFA, free fatty acid; SD, standard deviation

**Supplemental Table 8. Amounts of total free fatty acids, cholesterol and ChSO4 in the stratum corneum of the forearm from the patient and her parents: comparison with those of normal controls.**

| Total (ng/μg protein) | Patient (p.Arg276Cys homo) | Father (p.Arg276Cys hetero) | Mother (p.Arg276Cys hetero) | Controls, n=8 (mean±SD) |
|---|---|---|---|---|
| FFAs | 9.55 | 10.56 | 17.55 | 13.32±6.19 |
| Cholesterol | 17.69 | 14.33 | 17.77 | 10.09±2.09 |
| $ChSO_4$ | 1.12 | 0.58 | 0.92 | 0.51±0.10 |

Abbreviations: FFA, free fatty acid; SD, standard deviation

**Supplemental Table 9. Frequencies of *Sdr9c7* genotypes in pups derived from intercrosses between heterozygous mice.**

| +/+ | +/- | -/- | Total |
|---|---|---|---|
| 42 | 66 | 36 | 144 |

**Supplemental Table 10. List of locus and primers for potential off-target cleavage sites predicted by the CRISPOR.**

| Chrom | Locus | Primer sequence |
|---|---|---|
| chr8 | intergenic:Ces5a-Gm26843 | CTCGCGACAATTGACTGAAA<br>GAAGTGGTTGTCAAGCAGCA |
| chr15 | intron:Triobp | AGGTCCCTTTGGTGGGATAG<br>TTTGGATACAAAGCCCAAGG |
| chr12 | intergenic:Ttc6-Sstr1 | GGAACAGAAGCAAGGACGAA<br>ATCCCATCACTTGCAACACA |
| chr12 | intron:Ralgapa1 | CTCTACTCTGGGCGTTCAGG<br>AACCAACCAAACCCAAACAA |
| chr13 | intergenic:Zfp58-Zfp87 | CTCTGATCCTCTGGCACCTC<br>TACAGCCTGGCTAAGGGAGA |

**Supplemental Table 11. List of qPCR probes for mice used in this study.**

| Gene Symbol | Primer sequence | UPL number |
|---|---|---|
| *Alox12b* | ctttggtcctgatggcaac<br>gacaatcaggcccaggagt | #105 |
| *Aloxe3* | ggcctcactgatcttcaacg<br>gtccaggagacctcgaatctt | #4 |
| *Hprt1* | tgatagatccattcctatgactgtaga<br>aagacattctttccagttaaagttgag | #22 |
| *Lor* | ggttgcaacggagacaaca<br>catgagaaagttaagcccatcg | #11 |
| *Tgm1* | gcccttgagctcctcattg<br>cccttacccactgggatgat | #10 |
| *Sdr9c7* | caccaagtcggagaacgtc<br>ccattcgttgggaccact | #38 |
| *Irf4* | agcaccttatggctctctgc<br>tgactggtcaggggcataat | #3 |

Abbreviations: UPL, Roche Universal Probe Library

**Supplemental Table 12. The amount of endogenous d18:1/17:0 ceramide (NS_C35).**

| | | Peak area | | |
|---|---|---|---|---|
| | m/z | Synthetic standard-free sample (A) | Synthetic standard-added sample (B) | Ratio: (A)/(B)x100 |
| NS_C33 | 522.5 | 1124 | 710 | 158.3 |
| NS_C34 | 536.5 | 6065 | 2502 | 242.4 |
| **NS_C35** | **550.5** | **676** | **98023** | **0.69** |
| NS_C36 | 564.5 | 3093 | 2798 | 110.5 |
| NS_C37 | 578.6 | 322 | 886 | 36.3 |

**Supplemental Table 13. Selected m/z values for ceramide species (NH, AS, NDS) in the mass spectrometry analysis.**

| *m/z* value | Ceramide species | | |
|---|---|---|---|
| [M + acetate]- | NH retention time (min) | AS retention time (min) | NDS retention time (min) |
| 570.5 | | | NDS C32 16.5 |
| 584.5 | NH C32 14.1 | AS C32 16.0 | NDS C33 17.4 |
| 598.5 | NH C33 14.9 | AS C33 16.5 | NDS C34 18.3 |
| 612.5 | NH C34 15.6 | AS C34 17.1 | NDS C35 19.0 |
| 626.5 | NH C35 16.1 | AS C35 17.8 | NDS C36 19.6 |
| 640.5 | NH C36 16.9 | AS C36 18.4 | NDS C37 20.4 |
| 654.5 | NH C37 17.6 | AS C37 19.1 | NDS C38 21.2 |
| 668.6 | NH C38 18.3 | AS C38 19.8 | NDS C39 21.9 |
| 682.6 | NH C39 19.1 | AS C39 20.6 | NDS C40 22.7 |
| 696.6 | NH C40 19.7 | AS C40 21.4 | NDS C41 23.4 |
| 710.6 | NH C41 20.4 | AS C41 22.1 | NDS C42 24.2 |
| 724.6 | NH C42 21.1 | AS C42 22.8 | NDS C43 25.0 |
| 738.6 | NH C43 21.8 | AS C43 23.6 | NDS C44 25.7 |
| 752.6 | NH C44 22.6 | AS C44 24.3 | NDS C45 26.4 |
| 766.7 | NH C45 23.3 | AS C45 25.1 | NDS C46 27.1 |
| 780.7 | NH C46 24.1 | AS C46 25.8 | NDS C47 27.8 |
| 794.7 | NH C47 24.8 | AS C47 26.5 | NDS C48 28.5 |
| 808.7 | NH C48 25.5 | AS C48 27.2 | NDS C49 29.2 |
| 822.7 | NH C49 26.2 | AS C49 27.9 | NDS C50 29.7 |
| 836.7 | NH C50 27.0 | AS C50 28.5 | NDS C51 30.4 |
| 850.7 | NH C51 27.6 | AS C51 29.0 | NDS C52 31.0 |
| 864.8 | NH C52 28.1 | AS C52 29.6 | NDS C53 31.5 |
| 878.8 | NH C53 28.8 | AS C53 30.3 | NDS C54 32.1 |
| 892.8 | NH C54 29.5 | AS C54 31.0 | |

## Reference


1. Li H, Durbin R. Fast and accurate long-read alignment with Burrows-Wheeler transform. *Bioinformatics.* 2010;26(5):589-595.
2. Radner FP, et al. Growth retardation, impaired triacylglycerol catabolism, hepatic steatosis, and lethal skin barrier defect in mice lacking comparative gene identification-58 (CGI-58). *J Biol Chem.* 2010;285(10):7300-7311.
3. Hirabayashi T, et al. PNPLA1 has a crucial role in skin barrier function by directing acylceramide biosynthesis. *Nat Commun.* 2017;8:14609.
4. Thomas CP, Boeglin WE, Garcia-Diaz Y, O'Donnell VB, Brash AR. Steric analysis of epoxyalcohol and trihydroxy derivatives of 9-hydroperoxy-linoleic acid from hematin and enzymatic synthesis. *Chem Phys Lipids.* 2013;167-168:21-32.
5. Davis RW, Allweil A, Tian JH, Brash AR, Sulikowski GA. Stereocontrolled synthesis of four isomeric linoleate triols of relevance to skin barrier formation and function. *Tetrahedron Lett.* 2018;59(52):4571-4573.
6. Griffith WP, Ley SV. TPAP: Tetra-*n*-propylammonium perruthenate, a mild and convenient oxidant for alcohols. *Aldrichchimica Acta.* 1990;23(1):13 - 19.
7. Nugteren DH, Christ-Hazelhof E. Naturally-occurring conjugated octadecatrienoic acids are strong inhibitors of prostaglandin biosynthesis. *Prostaglandins.* 1987;33(3):403-417.
8. Hidalgo FJ, Zamora R, Vioque E. Syntheses and reactions of methyl (*Z*)-9,10-epoxy-13-oxo-(*E*)-11-octadecenoate and methyl (*E*)-9,10-epoxy-13-oxo-(*E*)-11-octadecenoate. *Chem Phys Lipids.* 1992;60(3):225-233.
9. Zheng Y, et al. Lipoxygenases mediate the effect of essential fatty acid in skin barrier formation: a proposed role in releasing omega-hydroxyceramide for construction of the corneocyte lipid envelope. *J Biol Chem.* 2011;286(27):24046-24056.
10. Chiba T, Thomas CP, Calcutt MW, Boeglin WE, O'Donnell VB, Brash AR. The Precise Structures and Stereochemistry of Trihydroxy-linoleates Esterified in Human and Porcine Epidermis and Their Significance in Skin Barrier Function: IMPLICATION OF AN EPOXIDE HYDROLASE IN THE TRANSFORMATIONS OF LINOLEATE. *J Biol Chem.* 2016;291(28):14540-14554.

11. Bligh EG, Dyer WJ. A rapid method of total lipid extraction and purification. *Can J Biochem Physiol.* 1959;37:911-917.
12. Hotz A, et al. Identification of mutations in SDR9C7 in six families with autosomal recessive congenital ichthyosis. *Br J Dermatol.* 2018;178(3):e207-e209.
13. Watanabe YS, et al. Anagliptin, a potent dipeptidyl peptidase IV inhibitor: its single-crystal structure and enzyme interactions. *J Enzyme Inhib Med Chem.* 2015;30(6):981-988.
14. Kartasova T, van de Putte P. Isolation, characterization, and UV-stimulated expression of two families of genes encoding polypeptides of related structure in human epidermal keratinocytes. *Mol Cell Biol.* 1988;8(5):2195-2203.
15. Jackson B, et al. Late cornified envelope family in differentiating epithelia--response to calcium and ultraviolet irradiation. *J Invest Dermatol.* 2005;124(5):1062-1070.
16. Masukawa Y, et al. Characterization of overall ceramide species in human stratum corneum. *J Lipid Res.* 2008;49(7):1466-1476.
17. van Smeden J, Hoppel L, van der Heijden R, Hankemeier T, Vreeken RJ, Bouwstra JA. LC/MS analysis of stratum corneum lipids: ceramide profiling and discovery. *J Lipid Res.* 2011;52(6):1211-1221.
18. Hsu FF, Turk J. Characterization of ceramides by low energy collisional-activated dissociation tandem mass spectrometry with negative-ion electrospray ionization. *J Am Soc Mass Spectrom.* 2002;13(5):558-570.
19. Masukawa Y, Tsujimura H, Narita H. Liquid chromatography-mass spectrometry for comprehensive profiling of ceramide molecules in human hair. *J Lipid Res.* 2006;47(7):1559-1571.
20. Yoo HH, Son J, Kim DH. Liquid chromatography-tandem mass spectrometric determination of ceramides and related lipid species in cellular extracts. *J Chromatogr B Analyt Technol Biomed Life Sci.* 2006;843(2):327-333.
21. Shaner RL, et al. Quantitative analysis of sphingolipids for lipidomics using triple quadrupole and quadrupole linear ion trap mass spectrometers. *J Lipid Res.* 2009;50(8):1692-1707.